12th National Conference on Earthquake Engineering
Salt Lake City, Utah
27 June - 1 July 2022
Hosted by the Earthquake Engineering Research Institute

Decision-Making Based on the Risk of Building Collapse due to Aftershock Hazard and Post-Earthquake Damage

A. M. Hulsey[1], F.A. Galvis[2], J.W. Baker[3], G.G. Deierlein[3]

ABSTRACT

This paper incorporates two decision-making frameworks for post-earthquake building evaluation and tagging: (1) guidelines for assessing damaged buildings based on their as-built collapse risk and post-earthquake damage and (2) criteria for time-dependent building reoccupancy decisions, considering the decaying aftershock hazard. These frameworks were previously proposed by other researchers as parallel concepts intended to complement each other. This paper links them explicitly, while updating the models based on related research advancements. The framework is demonstrated for buildings in downtown San Francisco, considering three mainshock earthquakes on the San Andreas Fault. A parametric study considers the potential range of collapse risk within a community's building inventory, based on the buildings' fundamental periods, their as-built (intact) capacity, and the decreased collapse capacity due to damage experienced during the earthquake, and the elapsed time (number of days) after the damaging earthquake. The results are presented in graphical form, describing the collapse risk at time, *t*, as a function of the original (intact) and reduced collapse capacity.

Introduction

Many studies have considered the post-earthquake, elevated risk of building collapse due to damage-induced reductions in collapse capacity and/or the increased aftershock hazard (e.g., [1]–[6]). While these studies all quantify the collapse risk, few engage the broader question of identifying the appropriate tagging threshold, at which to designate a building as safe (green tag) or unsafe (red tag) to reoccupy after the earthquake. Furthermore, while engineers can, by quantifying the risk, contribute to the discussion of acceptable risk levels, this question requires input from decision makers representing many stakeholders, considering the safety of building occupants within the broader context of post-earthquake recovery. Two studies, in particular, have described post-earthquake elevated risk of collapse in ways that facilitate these broader discussions. Bazzuro et al. [7] presented a graphical representation of recommended tagging criteria, including commentary on the (in)feasibility of red tagging an undamaged but poorly designed older building, whose collapse risk may be far higher than considered "acceptable." However, Bazzuro et al.'s study only considered the risk under steady-state hazard due to mainshocks, although it pointed to another study that considered the added risk due to increased aftershock activity. Yeo and Cornell [8] considered how to manage the building tagging decisions over time, recognizing that the elevated risk decreases as a function of time after the mainshock. This paper incorporates these two frameworks into one, using a graphical representation of the elevated risk at time, *t*, after the mainshock event. The following section describes the method for assessing the elevated hazard, based on Aftershock Probabilistic Seismic

[1] Research Fellow, Dept. of Civil & Env. Engineering, University of Auckland, New Zealand, 1023 (anne.hulsey@auckland.ac.nz)
[2] PhD Candidate, Dept. of Civil & Env. Engineering, Stanford University, California, 94305
[3] Professor, Dept. of Civil & Env. Engineering, Stanford University, California, 94305

Hulsey AM, Galvis FA, Baker JW, and Deierlein GG. Decision-Making Based on the Risk of Building Collapse due to Aftershock Hazard and Post-Earthquake Damage. *Proceedings of the 12th National Conference in Earthquake Engineering*, Earthquake Engineering Research Institute, Salt Lake City, UT. 2022.

Hazard Analysis (APHSA) and incorporating a few additional features based on subsequent research. The next section describes the risk assessment procedure for a parametric study of the potential range of buildings represented in the community. Finally, the results are presented graphically, showing the risk of collapse following a magnitude 7 event. These results are accompanied by a discussion of how the risk measures can help inform a transparent decision making process that considers the balance of meeting the community's post-earthquake recovery against the risk of building collapse.

Elevated Hazard Model, Considering both the Steady-State and Aftershock Hazard

The elevated hazard model is an extension of the APSHA model [9], which employs the same basic concepts as PSHA, where the rate of exceeding a shaking intensity (λ) is based on the rate of rupture event occurrences and the probability of exceeding the intensity given an event. APSHA adapts this framework by recognizing that the rate of aftershock event occurrence depends on the number of days since a mainshock event, as well as the magnitude and location of that mainshock. The elevated hazard model includes both the steady-state hazard (λ_{ss}, time independent) and aftershock hazard (λ_a, decaying with time) by summing the rate of exceedance from both contributions. The hazard is calculated at time t after the mainshock, considering the following time period of Δt days. In this study, Δt =30 days, requiring the time independent steady-state hazard to be converted from the typical mean annual rate to a mean monthly rate. The result is an elevated hazard (λ_e) immediately following the mainshock that decays back to the steady-state over time. The initial increase and the time until the hazard returns to the steady-state depend on the magnitude of the conditioning mainshock, based the Reasenberg and Jones aftershock model [10].

This paper's case study implements two additional features as compared to the original APSHA method. First, the Reasenberg and Jones model's generic parameters for California aftershock environments are updated based on the generic Northern California parameters from a more recent study for four regions within California [11]. Second, the shaking intensity measure is defined as the average spectral acceleration, $Sa_{avg}(T)$, where T is the fundamental period of the building under consideration and the spectral acceleration values are averaged over the range $0.2 - 3.0\,T$. This intensity measure better accounts for the spectral shape of ground motions when assessing a building's collapse capacity [12], [13]. In this study, $Sa_{avg}(T)$ is calculated using the Chiou and Youngs ground motion model [14], which includes an aftershock flag to reflect the difference in predicted ground motions between mainshock and aftershock events. The result is an elevated hazard curve for $Sa_{avg}(T)$ that considers ground motions from both mainshock (as part of the steady-state hazard) and aftershock events. The left axis of Figure 1a shows the elevated hazard curve (λ_e, solid pink) at 10 days after a magnitude 7 mainshock ($m_m = 7$), along with the steady-state hazard (λ_{ss}, dashed black).

Parametric Study for the Potential Range of Buildings in the Community

Building tagging decisions are intended to reflect the post-earthquake collapse risk of buildings. Risk assessments depend on two features: hazard and exposure. The previous section accounted for the elevated hazard following a mainshock. This section considers the exposure, using a parametric study to consider a range of buildings in the community. The three considered parameters are the building's fundamental period, T, the collapse probability target of the as-built (intact) building, and the reduced collapse capacity due to earthquake-induced damage. The period, T, determines the intensity measure for the building, $Sa_{avg}(T)$. The concept is illustrated in Figure 1a, where the left axis refers to the steady-state (black dashed) and elevated (solid pink) $Sa_{avg}(T)$ hazard for T = 1.0 second. The dotted line indicates the benchmark intensity, set as the 2% in 50 year intensity for the steady-state hazard, roughly 0.55g for the T = 1.0 second hazard.

The benchmark intensity is combined with a collapse probability target to determine the median collapse capacity of the intact building, $\widehat{Sa}_{collapse}^{Intact}$, where the right axis of Figure 1a refers to the collapse fragility (solid blue). The figure demonstrates a "benchmark point" (indicated by an X) with a collapse probability target of $P\left(C\middle|Sa_{2\%in50yr}\right) = 10\%$. The collapse fragility passes through this point with a log standard deviation of β = 0.6. This parametric study uses $P\left(C\middle|Sa_{2\%in50yr}\right) = 10\%$ as a proxy for a building designed to code. However, the community may also include better-than-code buildings with a lower collapse probability or older buildings with a higher collapse probability. These are represented by the range $2.5\% \le P\left(C\middle|Sa_{2\%in50yr}\right) \le 50\%$. Finally, the reduced collapse capacity due to damage experienced during the mainshock is characterized as a fraction of the intact collapse capacity, i.e.,

$\kappa = \widehat{Sa}_{collapse}^{Damaged} / \widehat{Sa}_{collapse}^{Intact}$. The study considers $0.8 \leq \kappa \leq 1.0$ for moderate to no reduction in the collapse capacity.

The elevated risk of collapse is calculate using the risk convolution equation [15]. The hazard curve depends on the building period and the time t following a mainshock with magnitude m_m. The collapse fragility depends on the intact collapse capacity and reduced collapse capacity. The risk is quantified as a multiple of the "code risk", or the steady-state risk for an intact building, $\kappa = 1.0$, benchmarked to the proxy for code-based design: $P\left(C\middle|Sa_{2\%in50yr}\right) = 10\%$. Figure 1b shows the risk of collapse for the intact, $T = 1.0$ second building represented by the blue collapse fragility in Figure 1a. The black dashed line corresponds to the steady-state collapse risk, with a Risk Multiplier = 1.0. The x-axis reflects the decaying hazard as t increases, considering the month following t (Δt =30). The purple, pink, and maroon colors depict the risk to a building in downtown San Francisco, following mainshocks on the San Andreas Fault (13km from the site) with magnitudes $m_m = 6.5, 7$, and 8, respectively. The solid lines show the elevated risk of collapse, calculated as the sum of the collapse risk due to the steady-state hazard (dashed black) and aftershock hazard (dotted). The next section will discuss the results for additional collapse probability targets and reduced collapse capacities.

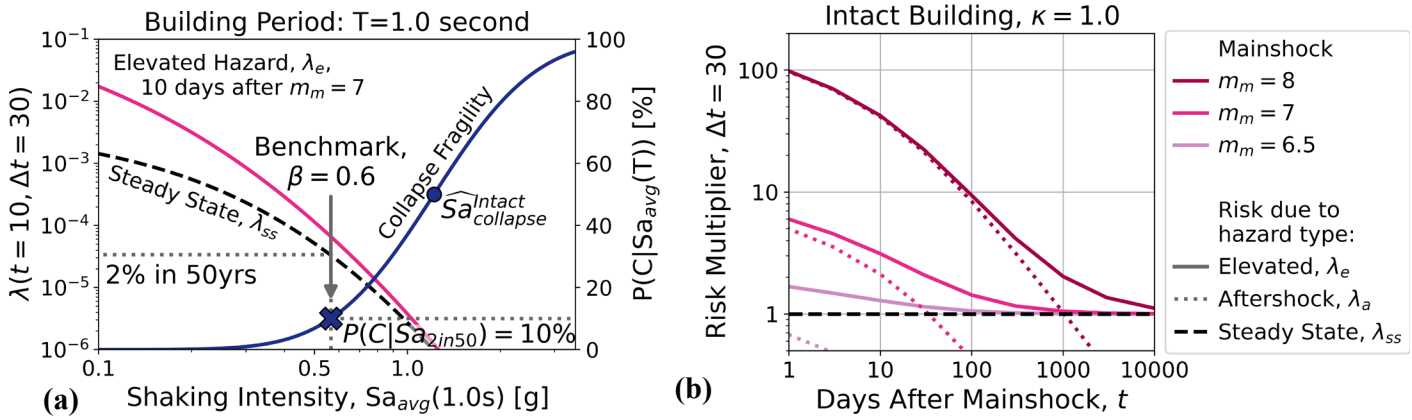

Figure 1: Example of the collapse risk assessment for a building in the parametric study. **(a)** The steady-state (dashed black) and elevated (solid pink) hazard curves for a fundamental building period of T=1.0 second. The median collapse capacity for the intact building ($\widehat{Sa}_{collapse}^{Intact}$, blue circle) represents a collapse fragility with a log standard deviation of $\beta = 0.6$ passing through the benchmark point (blue X) set as a proxy for code-based design: a 2% in 50 year intensity and a collapse probability target of $P\left(C\middle|Sa_{2\%in50yr}\right) = 10\%$. **(b)** The risk of collapse for an intact building, quantified as a multiple of the "code risk": the steady-state risk for a building with $P\left(C\middle|Sa_{2\%in50yr}\right) = 10\%$. The risk is a function of the magnitude of the mainshock, m_m, the time after the mainshock, t, and the time period considered (Δt =30). The purple, pink, and maroon solid lines show the elevated collapse risk for mainshock magnitudes of 6.5, 7, and 8, respectively. The dotted lines show the risk contribution due to the aftershock hazard, in comparison to the steady-state contribution (dashed black).

Graphical Representation of Elevated Collapse Risk

The results of the parametric study are presented in graphical form in Figure 2. The building period is held fixed ($T = 1$ second), while the x-axis spans the collapse probability targets and the y-axis spans the reduced collapse capacity due to damaged experienced during the mainshock. Figure 2a is based on the elevated collapse risk at 10 days after a mainshock with $m_m = 7$ and Figure 2b shows steady-state collapse risk (equivalent to the elevated collapse risk at 1000 days, see Figure 1b). The risk is quantified as a Risk Multiplier (RM) of the "code risk", as described above. Note that the steady-state contour for RM = 1 (Figure 2b) passes through $P\left(C\middle|Sa_{2\%in50yr}\right) = 10\%$ and $\kappa = 1.0$ as the proxy for code-based design. These RM values are further depicted as colored recoccupancy (tagging) criteria, shown here for commercial office buildings with green for RM ≤ 3 and red for RM ≥ 6 [8]. While these criteria are assumed to be reasonable for illustrating the process, the purpose of this study is to facilitate discussion among stakeholders to identify the appropriate tagging thresholds based on the community's values. These stakeholder discussions will allow for a more transparent decision-making process. For example, the acceptable risk criteria may be adjusted for older,

poorly designed buildings, reflecting a trade-off between the benefit to building inhabitants (example returning to work or a place of residence) versus the increased life-safety risk associated with building collapse. Similarly, the criteria may change following a mainshock with $m_m = 8$ as compared to $m_m = 7$, to allow re-entry into some of the community's buildings, despite the significantly higher collapse risk (see Figure 1b). All these factors can be discussed based on the community's unique values and priorities with respect to life-safety risks and maintaining building access.

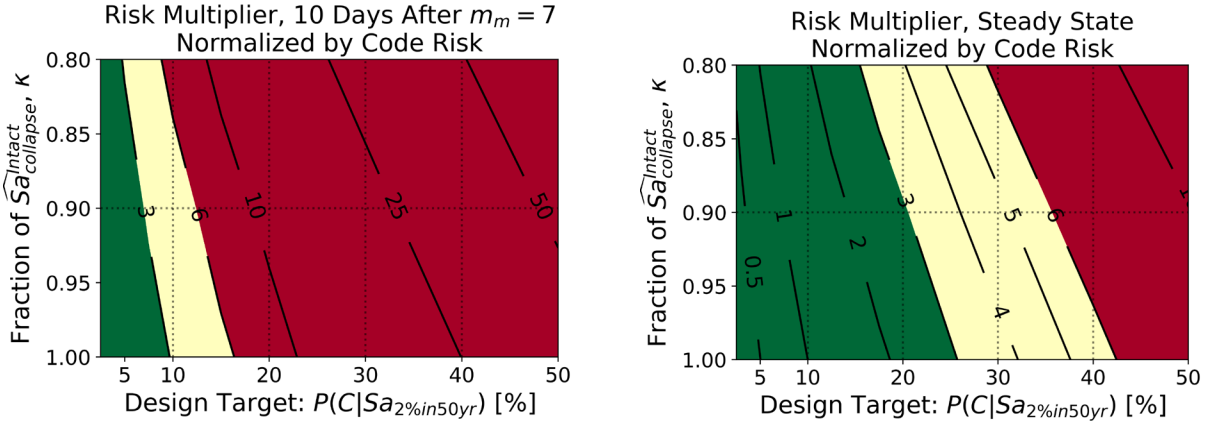

Figure 2: Graphical representation of the collapse risk for buildings with $T = 1$ second, considering a range of design targets, $P(C|Sa_{2\%in50yr})$, and post-mainshock damage, κ. The risk multiplier contours show the multiple of the "code risk", with $P(C|Sa_{2\%in50yr}) = 10\%$ and $\kappa = 1.0$. The colors help visualize the variation, with RM ≤ 3 show in green and RM ≥ 6 shown in red. **(a)** Risk multipliers for the steady-state risk. **(b)** Risk multipliers 10 days after a magnitude 7 event.

Conclusions

The proposed framework builds on previous work to graphically represent the risk of collapse for a range of post-earthquake building conditions. These conditions include (1) the elevated yet decaying hazard following a mainshock event, (2) the building period, (3) the collapse risk of the as-built, intact building, and (4) the reduced collapse capacity due to damage accrued during the mainshock event. The graphical representation facilitates a risk-informed decision-making process, allowing decision makers to adjust the post-earthquake reoccupancy (tagging) criteria for older buildings or the increased aftershocks following larger magnitude events as necessary for balancing the post-earthquake needs of building occupants against the risk of collapse.

Acknowledgments

The first author would like to thank Dr. Ganyu Teng for a short but significant conversion regarding combining the aftershock and steady-state hazard into a single, elevated hazard model. Funding for this project was provided by a Stanford Graduate Fellowship, the EERI/FEMA NEHRP Graduate Fellowship, and the Achievement Reward for College Scientists (ARCS) Scholar Fellowship.

References

[1] N. Luco, P. Bazzurro, and C. A. Cornell, "Dynamic Versus Static Computation Of The Residual Capacity Of A Mainshock-damaged Building To Withstand An Aftershock," 2004.

[2] J. Ruiz-García and J. D. Aguilar, "Aftershock seismic assessment taking into account postmainshock residual drifts," *Earthquake Engineering & Structural Dynamics*, vol. 44, no. 9, pp. 1391–1407, Jul. 2015, doi: 10.1002/eqe.2523.

[3] M. Raghunandan, A. B. Liel, and N. Luco, "Aftershock collapse vulnerability assessment of reinforced concrete frame structures," *Earthquake Engineering & Structural Dynamics*, vol. 44, no. 3, pp. 419–439, Mar. 2015, doi: 10.1002/eqe.2478.

[4] H. v. Burton and G. G. Deierlein, "Integrating visual damage simulation, virtual inspection, and

collapse capacity to evaluate post-earthquake structural safety of buildings," *Earthquake Engineering & Structural Dynamics*, vol. 47, no. 2, pp. 294–310, 2018, doi: 10.1002/eqe.2951.

[5] A. M. Hulsey, "The Regional Impact of Post-Earthquake Safety Decisions Based on Damage to Tall Buildings and Elevated Hazard Due to Aftershocks," 2020.

[6] FEMA-352, "Recommended Postearthquake Evaluation and Repair Criteria for Welded Steel Moment-Frame Buildings, SAC Joint Venture," 2000. Accessed: Apr. 17, 2017. [Online]. Available: http://mitigation.eeri.org/files/fema-352.pdf

[7] P. Bazzurro, C. A. Cornell, C. Menun, and M. Motahari, "Guidelines For Seismic Assessment Of Damaged Buildings," 2004. Accessed: Mar. 12, 2017. [Online]. Available: http://www.iitk.ac.in/nicee/wcee/article/13_1708.pdf

[8] G. L. Yeo and C. A. Cornell, "Building Tagging Criteria Based On Aftershock PSHA," 2004. Accessed: Mar. 15, 2017. [Online]. Available: http://www.iitk.ac.in/nicee/wcee/article/13_3283.pdf

[9] G. L. Yeo and C. A. Cornell, "A probabilistic framework for quantification of aftershock ground-motion hazard in California: Methodology and parametric study," *Earthquake Engineering & Structural Dynamics*, vol. 38, no. 1, pp. 45–60, Jan. 2009, doi: 10.1002/eqe.840.

[10] P. A. Reasenberg and L. M. Jones, "Earthquake hazard after a mainshock in California," *Science*, vol. 243, no. 4895, pp. 1173–1176, 1989, doi: 10.1126/science.243.4895.1173.

[11] J. L. Hardebeck, A. L. Llenos, A. J. Michael, M. T. Page, and N. van der Elst, "Updated California aftershock parameters," *Seismological Research Letters*, vol. 90, no. 1, pp. 262–270, 2019, doi: 10.1785/0220180240.

[12] P. P. Cordova, G. G. Deierlein, S. S. Mehanny, and C. A. Cornell, "Development of a Two-Parameter Seismic Intensity Measure and Probablistic Assessment Procedure," in *The Second US-Japan Workshop on Performance-Based Earthquake Engineering Methodology for Reinforced Concrete Building Structures*, 2000, pp. 187–206.

[13] M. Kohrangi, P. Bazzurro, and D. Vamvatsikos, "Vector and Scalar IMs in Structural Response Estimation, Part I: Hazard Analysis," *Earthquake Spectra*, vol. 32, no. 3, pp. 1507–1524, Aug. 2016, doi: 10.1193/053115EQS080M.

[14] B. S. J. Chiou and R. R. Youngs, "An NGA Model for the Average Horizontal Component of Peak Ground Motion and Response Spectra," *Earthquake Spectra*, vol. 24, no. 1, pp. 173–215, 2008, doi: 10.1193/1.2894832.

[15] H. Krawinkler, F. Zareian, R. A. Medina, and L. F. Ibarra, "Decision support for conceptual performance-based design," *Earthquake Engineering and Structural Dynamics*, vol. 35, no. 1, pp. 115–133, 2006, doi: 10.1002/eqe.536.